MATHEMATICAL BIOSCIENCES
AND ENGINEERING
Volume **9**, Number **1**, January **2012**

doi:10.3934/mbe.2012.9.199

pp. **199–214**

EFFECT OF BRANCHINGS ON BLOOD FLOW IN THE SYSTEM OF HUMAN CORONARY ARTERIES

Benchawan Wiwatanapataphee

Department of Mathematics, Faculty of Science
Mahidol University, Bangkok 10400, Thailand
Centre of Excellence in Mathematics, PERDO, CHE, Thailand

Yong Hong Wu

Department of Mathematics and Statistics
Curtin University of Technology, Perth, WA 6845, Australia

Thanongchai Siriapisith

Department of Radiology, Faculty of Medicine Siriraj Hospital
Mahidol University, Bangkoknoi, Bangkok, 10700, Thailand

Buraskorn Nuntadilok

Department of Mathematics, Faculty of Science
Mahidol University, Bangkok 10400, Thailand

(Communicated by Qing Nie)

Abstract. In this work, we investigate the behavior of the pulsatile blood flow in the system of human coronary arteries. Blood is modeled as an incompressible non-Newtonian fluid. The transient phenomena of blood flow through the coronary system are simulated by solving the three dimensional unsteady state Navier-Stokes equations and continuity equation. Distributions of velocity, pressure and wall shear stresses are determined in the system under pulsatile conditions on the boundaries. Effect of branching vessel on the flow problem is investigated. The numerical results show that blood pressure in the system with branching vessels of coronary arteries is lower than the one in the system with no branch. The magnitude of wall shear stresses rises at the bifurcation.

1. **Introduction.** The major vessels of the coronary circulation as shown in Fig. 1 are the left coronary (LCA) that divides into left anterior descending (LAD) and circumflex branches (LCX), and the right coronary artery (RCA). The left and right coronary arteries originate at the base of the aorta and lie on the surface of the heart. Through these vessels, blood is distributed to different regions of the heart muscle. As one gets older, vessels may become hardened and contain fatty deposits or atheromas on the inner lining of the vessel. This reduces the vessel's ability to expand during the systole. The deposition of atheromas in the arteries causes narrowing of the coronary arteries known as the coronary artery disease (CAD). These arterial changes occur silently, and symptoms are often present only until atheromas occlude more than two thirds of the vessel [32]. Fig. 2 shows a conventional angiogram of a stenosed coronary artery with an arrow pointing to the stenosis at the proximal part of the RCA.

2000 *Mathematics Subject Classification.* Primary: 92C10; Secondary: 92C50.
Key words and phrases. Mathematical modelling, blood flow, human coronary artery.

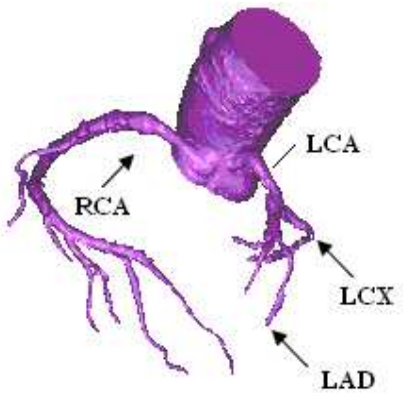

FIGURE 1. The major vessels of the coronary circulation

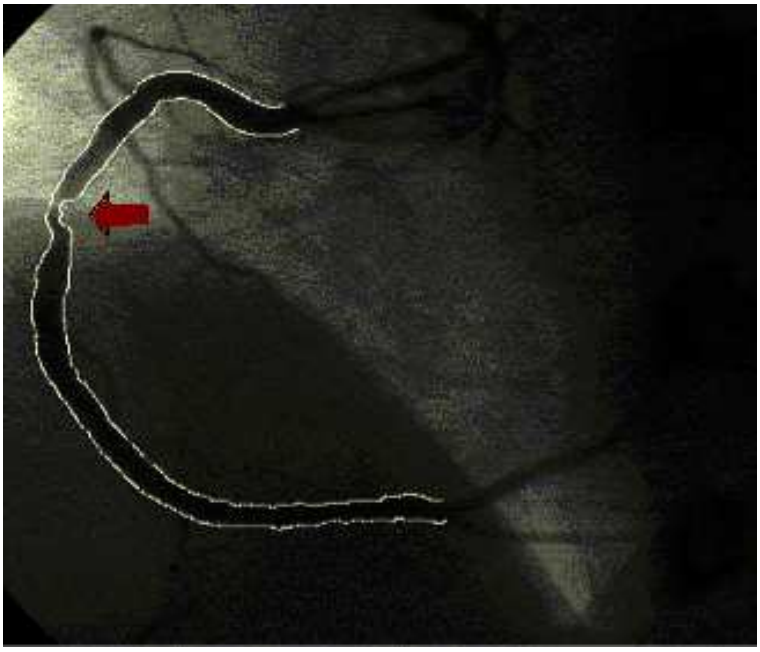

FIGURE 2. The angiogram of the RCA with stenosis. The arrow in the figure points to the stenosis.

Today the CAD is considered as one of the major causes of human death. Most of the cases are associated with some form of abnormal blood flow in arteries due to the existence of stenoses. To create a new pathway for blood flow, the technique of coronary artery bypass grafting (CABG) has been widely used for patients with severe coronary artery diseases. In a CABG operation, the surgeon grafts the patient own blood vessels, such as veins from the legs or arteries from the chest or arms, onto the diseased coronary artery.

Over the last two decades, a large number of bypass grafts have been implanted worldwide. However, up to 25 percents of grafts fail within one year and up to 50 percents fail within ten years after surgery [33]. Today, it has been recognized that one of the most important determinations in a successful bypass operation is the information of the rheological behavior of blood, the flow speed, the pressure distribution, the wall shear stress, and the wall deformation in cardiac cycles. Thus over the last two decades, extensive research has been carried out to study blood flow problems in the coronary artery, including experimental, analytical and numerical studies. Studies for both normal and stenotic vessels have been carried out for idealized arteries, idealized arterial bifurcations, branchings, and for specific, clinically important cases such as the aortic arch, the carotid artery, and the coronary arteries. In most work, blood is assumed to be a Newtonian fluid which is generally a valid approximation for the rheological behavior of blood in the large blood vessels with diameter of 2-3 millimeters [23, 26, 35]. Fei et al. [26] constructed three dimensional iliofermoral bypass graft distal anastomoses under various conditions of anastomotic angle configurations of 20, 30, 40, 45, 50, 60 and 70 degree. The flow patterns and wall shear stress were numerically simulated. Staalsen et al. [35] performed the end-to-side anastomosis with polyurethane graft on the pig abdominal aorta.

To investigate the relationship between hemodynamic effect of the blood circulation and vascular diseases in small vessels, the non-Newtonian effect of the blood has been considered [22, 28, 29, 39]. Basombrio et al. [22] constructed numerical experiments for non-trivial flow, close to realistic situations in hemodynamics. The non-Newtonian effect based on the Casson's rheological model was included. Jie et al. [28] also included the effect of non-Newtonian property of blood in the model. They investigated the influence of the non-Newtonian property of fluid on the wall shear stress and flow phenomena. It is noted that the studies mentioned above used totally unrealistic boundary conditions, such as constant velocity at the inlet and constant pressure at the outlet. In 2006, Wiwatanapataphee et al. [39] studied the effect of the bypass graft angle on the blood flow. They simulated the three-dimension unsteady non-Newtonian blood flow in the artificial artery bypass graft using realistic boundary conditions arising from the heart pump. The effect of using different bypass graft angles, 45^o, 60^o and 90^o, on the flow pattern was investigated in that study.

In this work, we extend our previous work [39] on two aspects. Firstly, the computational model is constructed based on the real geometry of human coronary arteries by using CT scans. Secondly, the model includes the aorta, the left and the right coronary arteries, and mimics the pulsatile flow condition. In comparison with previous work, these two new features represent a significant advance toward the application of mathematical model in surgery, as the model with these features enable the computation of blood distribution to each part of the coronary artery system so as for doctors to determine the critical conditions for surgery. It also provides a computer-aided means for doctors to design the geometry of bypass grafts if necessary.

The rest of this paper is organized as follows. In section two, the complete set of governing equations for blood flow is presented. In section three, a Bubnov-Galerkin finite element method and numerical scheme for the solution of the problem is formulated. In section four, numerical simulations for flow through the coronary

artery are shown. Finally some conclusions and the clinical significance of the results are presented in section five.

2. **Mathematical model.** The reliability of a robust mathematical model for simulating blood flow in the coronary artery system depends on the proper construction of the three essential components: the geometry of the system, the flow mechanism and relevant boundary conditions, and the underlying differential equations governing the dynamics of the flow.

The construction of the computation domain of the system of human coronary arteries is based on over four hundreds computed tomography (CT) images of a patient. CT scan data is converted to Stereolithography (STL) format and saved in a file by the MIMIC software. From the CT image data, we obtain the real geometry of many cross-sections of the aorta and RCA as well as LCA branches. These cross-section boundaries are smoothed using B-spline curves [3, 38] and then are superimposed perpendicularly onto the central lines of the aorta and RCA/LCA branches to form the 3-D domain. Figure 3 shows the 3-D geometry of the system of human coronary arteries.

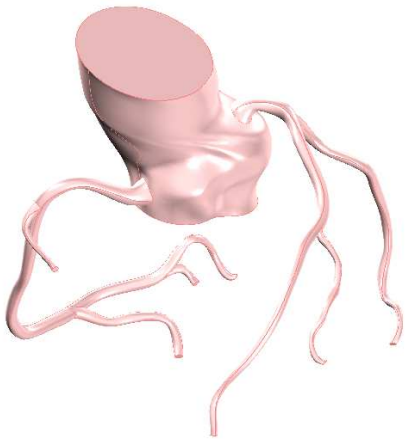

FIGURE 3. Geometry of the system of human coronary arteries.

For the dynamics of blood flow, we assume blood as an incompressible non-Newtonian fluid. The governing equations of blood flow consist of the continuity equation and the Navier-Stokes equations, which can be expressed in vector notation as follows:

$$\nabla \cdot \mathbf{u} = 0 \quad \text{in } \Omega_1, \tag{1}$$

$$\frac{\partial \mathbf{u}}{\partial t} + (\mathbf{u} \cdot \nabla)\mathbf{u} = \frac{1}{\rho}\nabla \cdot \sigma \quad \text{in } \Omega_1, \tag{2}$$

where $\mathbf{u}$ is the blood velocity vector in the lumen region, ρ is the density of blood, σ is the total stress tensor which is defined by

$$\sigma = -pI + 2\eta(\dot{\gamma})\mathbf{D}, \tag{3}$$

where p is the pressure and D is the rate of deformation tensor given by

$$\mathbf{D} = \frac{1}{2}\left(\nabla\mathbf{u} + (\nabla\mathbf{u})^T\right),$$

in which η and $\dot{\gamma}$ denote respectively the viscosity of blood and shear rate. Various non-Newtonian models have been proposed to describe the relation between η and $\dot{\gamma}$. In this work, we use Carreau's shear-thinning model, namely,

$$\eta = \eta_\infty + (\eta_0 - \eta_\infty)\left[1 + (\lambda\dot{\gamma})^2\right]^{(n-1)/2},$$

in which the zero shear viscosity η_0 and the infinite shear viscosity η_∞ are set to be 0.56 and 0.0345 $(dyne/cm^2)\cdot s$, respectively; a model parameter λ is set to be 3.313 s and the consistency index n is a parameter whose value is 0.3568; $\dot{\gamma} = \sqrt{2tr(\mathbf{D}^2)}$ is a scalar measure of the rate of deformation tensor:

$$\dot{\gamma} = \sqrt{2u_{1_x}^2 + 2u_{2_y}^2 + 2u_{3_z}^2 + (u_{1_y} + u_{2_x})^2 + (u_{2_z} + u_{3_y})^2 + (u_{1_z} + u_{3_x})^2}.$$

In the human cardiovascular system, due to the pulsatile pressure created by the heart pump, blood is pushed from aorta to the left and the right coronary arteries from which blood is distributed to different part of the heart muscle. In most existing model, the computational region is limited to one artery and the flow rate to this artery is fixed, which obviously does not describe the real situation. Thus, in this work, we construct the model consisting of the aorta, the RCA and the LCA, with which the flow rate on the entry of the aorta is specified while the flow rate to the RCA and The LCA is allowed to be determined based on the system configuration and the flow condition which is more realistic and allow determination of flow behaves under different conditions. As blood is pumped into the aorta with a fixed pulsatile flow rate and is distributed to different branches and exits, we set the condition on the entry of the aorta as pulsatile velocity boundary condition, and the condition on the exits of arteries as pressure boundary condition, while the conditions on the blood-vessel wall are non-slip boundary condition.

Thus, on the entry of aorta, the velocity is set to the pulsatile velocity

$$\bar{u}_{in}(t) = Q(t)/A, \tag{4}$$

where A and $Q(t)$ are the cross-section area of the inlet surface and the pulsatile flow rate. The typical pressure and flow rate profiles in different parts of the arterial system are as shown in figure 4. According to reference [39], the flow waveform can be expressed by the following Fourier series:

$$Q(t) = \overline{Q} + \sum_{n=1}^{4} \alpha_n^Q cos(n\omega t) + \beta_n^Q sin(n\omega t). \tag{5}$$

On the exits, the pulsatile condition is used. According to [39], the pulsatile pressure takes the form of the following Fourier series:

$$p(t) = \overline{p} + \sum_{n=1}^{4} \alpha_n^p cos(n\omega t) + \beta_n^p sin(n\omega t), \tag{6}$$

where $\bar{Q}$ is the mean volume flow rate, $\omega = \dfrac{2\pi}{T}$ is the angular frequency with period $T = 0.8$s and $\bar{p}$ is the mean pressure. Thus, on the outlet boundary, the boundary condition is

$$\sigma \cdot \mathbf{n} = -p(t)\mathbf{n}, \tag{7}$$

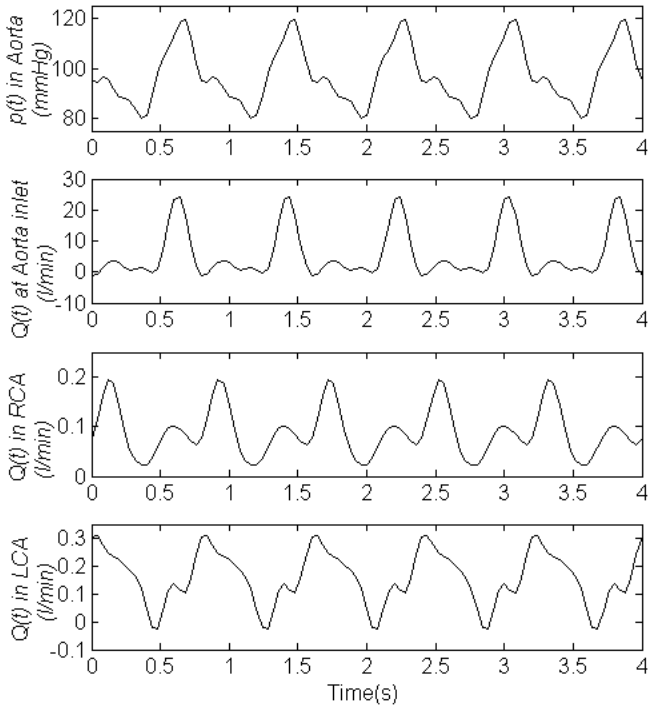

FIGURE 4. The periodic blood pressure and flow rate waveforms oscillating within systolic and diastolic levels with cardiac period $T = 0.8s$.

TABLE 1. Values of the parameters α_n^Q, α_n^p, β_n^Q and β_n^p

Artery vessel	n	α_n^Q	β_n^Q	α_n^p	β_n^p
Aorta	1	1.7048	-7.5836	8.1269	-12.4156
$\bar{Q} = 5.7222$	2	-6.7035	-2.1714	-6.1510	-1.1072
$\bar{p} = 97.2222$	3	-2.6389	2.6462	-1.333	-0.3849
$A = 6.7287$	4	0.7198	0.2687	-2.9473	1.1603
LCA	1	0.1007	0.0764	-3.3107	-2.2932
$\bar{Q} = 0.1589$	2	-0.0034	-0.0092	-9.8639	8.0487
$\bar{p} = 84.9722$	3	0.0294	0.0337	3.0278	3.8009
	4	0.0195	-0.0129	2.2476	-3.2564
RCA	1	0.0393	0.0241	5.9369	3.6334
$\bar{Q} = 0.0896$	2	-0.0360	0.0342	-11.1997	2.1255
$\bar{p} = 95.3333$	3	-0.0131	0.0026	-2.2778	-3.7528
	4	-0.0035	-0.0041	2.7333	-0.6375

where $\mathbf{n}$ is the outward unit normal vector at the boundary. No-slip condition is applied to the outer arterial wall. The values of $\bar{Q}$, $\bar{p}$, α_n^Q, α_n^p, β_n^Q and β_n^p are as shown in Table 1.

In summary, the blood flow problem in the system of human coronary arteries is governed by the following boundary value problem.

BVP: Find $\mathbf{u}$ and p such that equations (1)-(2) and all boundary conditions are satisfied.

3. **Numerical algorithm based on the finite element method.** To develop a variational statement corresponding to the BVP, we consider the following alternative problem:
Find $\mathbf{u} \in [H^1(\Omega)]^3$, and $p \in H^1(\Omega)$ such that for all $\mathbf{w}^u \in [H_0^1(\Omega)]^3$, and $w^p \in H_0^1(\Omega)$, all boundary conditions are satisfied and

$$\begin{gathered}(\nabla \cdot \mathbf{u}, w^p) = 0, \\ \left(\frac{\partial \mathbf{u}}{\partial t}, \mathbf{w}^u\right) + ((\mathbf{u} \cdot \nabla)\mathbf{u}, \mathbf{w}^u) = \frac{1}{\rho}\left(\nabla \cdot [-pI + \eta(\nabla \mathbf{u} + (\nabla \mathbf{u})^T)], \mathbf{w}^u\right),\end{gathered} \tag{8}$$

where $H^1(\Omega)$ is the Sobolev space $W^{1,2}(\Omega)$ with norm $\|\cdot\|_{1,2,\Omega}$ and $H_0^1(\Omega) = \{v \in H^1(\Omega) | v = 0$ on the Dirichlet type boundary$\}$, and $(\cdot, \cdot)$ denotes the inner product on the square integrable function space $L^2(\Omega)$.

By using the boundary conditions (4) and (7) and applying the standard procedures for the development of the Galerkin finite element formulation, we obtain the following system

$$\begin{aligned} C^T \mathbf{U} &= 0, \\ M\dot{\mathbf{U}} + D_u(u)\mathbf{U} + \widehat{C}P &= 0, \end{aligned} \tag{9}$$

where $\mathbf{U} = (\underline{u}_1, \underline{u}_2, \underline{u}_3, ..., \underline{u}_N)$ with $\underline{u}_i$ being the velocity vector at the ith finite element node; the matrices C, M, $D_u(u)$ and $\widehat{C}$ are derived in the Galerkin finite element formulation but are not presented here to keep details of the paper to minimum.

In the present study, we solve the system of equation (9) using an implicit time integration scheme. For a typical time step $(t_n \to t_{n+1})$, we have

$$\begin{aligned} C^T \mathbf{U}_{n+1} &= 0, \\ \left(\frac{M}{\Delta t_n} + D_u(u)\right)\mathbf{U}_{n+1} + \widehat{C}P_{n+1} &= \frac{M}{\Delta t_n}\mathbf{U}_n, \end{aligned} \tag{10}$$

which is nonlinear because D_u depends on $\mathbf{U}_{n+1}$. To deal with this nonlinearity for an iterative solution of (10), we use the following iterative updating:

$$\begin{aligned} C^T \mathbf{U}_{n+1}^{i+1} &= 0, \\ \left(\frac{M}{\Delta t_n} + D_{n+1}^i\right)\mathbf{U}_{n+1}^{i+1} + \widehat{C}P_{n+1}^{i+1} &= \frac{M}{\Delta t_n}\mathbf{U}_n^i, \end{aligned} \tag{11}$$

where the superscript i denotes evaluation at the ith iteration step. Therefore, in a typical time step $(t_n \to t_{n+1})$, starting with $\mathbf{U}_{n+1}^0 = \mathbf{U}_n$ we determine $\mathbf{U}_{n+1}^{i+1}$ and P_{n+1}^{i+1} by solving system (11) repeatedly until $\left\|\mathbf{U}_{n+1}^{i+1} - \mathbf{U}_{n+1}^i\right\| < \varepsilon_u$ and $\left\|P_{n+1}^{i+1} - P_{n+1}^i\right\| < \varepsilon_p$. In this study, ε_u and ε_p are set to be 0.001.

By repeatedly using the above procedure for $n = 0, 1, 2, \ldots$ we can determine the state $\mathbf{U}$ and P of the system at $t_0, t_1, t_2, \ldots$. If the norm $\|\mathbf{U}_{n+1} - \mathbf{U}_n\|$ and $\|P_{n+1} - P_n\|$, are sufficiently small, then the system approaches the so-called steady state.

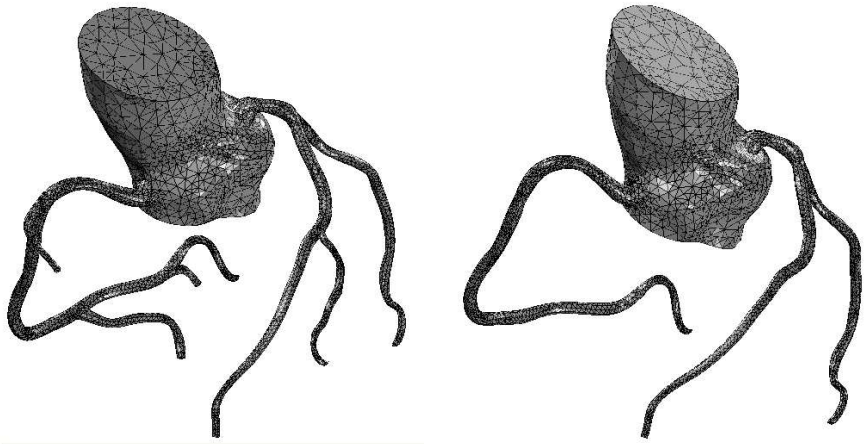

(a) (b)

FIGURE 5. The finite element mesh of the three-dimensional coronary artery: (a) with branches; (b) with no branch.

4. **Results and discussion.** We have simulated the three-dimensional blood flow through the system of coronary artery with branches and with no branch. The computation region, as shown in Figure 3, represents the system of human coronary arteries. The system of the coronary arteries consists of the right coronary artery (RCA) and the left coronary artery (LCA) which typically runs for 1 to 25 mm and then bifurcates into the left anterior descending (LAD) artery and the left circumflex artery (LCX) [1]. In this study, the volume and surface area of the coronary system are 30.872 cm^3 and 82.615 cm^2. The area and perimeter of the inlet aorta are 6.712 cm^2 and 9.893 cm. The area and perimeter of the exit boundary of the aorta are 8.0243 cm^2 and 10.0559 cm. The lengths of the RCA, the LAD and the LCX are 14.9215 cm, 8.7269 cm and 8.2293 cm, respectively.

Flow simulations were conducted under typical physiological conditions. The fluid properties are typical of human blood with the density of 1.06 $g \cdot cm^{-3}$ [37]. The mean flow rate ($\bar{Q}$) and mean pressure ($\bar{p}$) of the aorta are equal to 5.7222 $l \cdot min^{-1}$ and 97.2222 mmHg, respectively. Two finite element meshes of the system with and with no branch are shown in Figure 5 consisting of 15,510 tetrahedral elements with 121,194 degrees of freedom and 13,106 tetrahedral elements with 104,019 degrees of freedom, respectively.

Figure 6 illustrates the pressure field in a cardiac cycle at various points in the system with branches. It is noted that the pressure decreases linearly along the arterial axis. Figure 7 shows the vector plot of the blood flow in the system with branches at the peak of the systole. It shows that the blood passes through the RCA at 40 cm/sec at the beginning section originating from the aorta of the heart and at 5 cm/sec at the end section of the RCA. When it arrives at the bifurcation, it splits into two parts. This reduces the pressure along the artery line while the magnitude of wall shear stresses rises at the bifurcation as shown in figures 13(a) and 14(a). The results indicate that artherosclerotic lessions is likely to develop around the branchings of the artery.

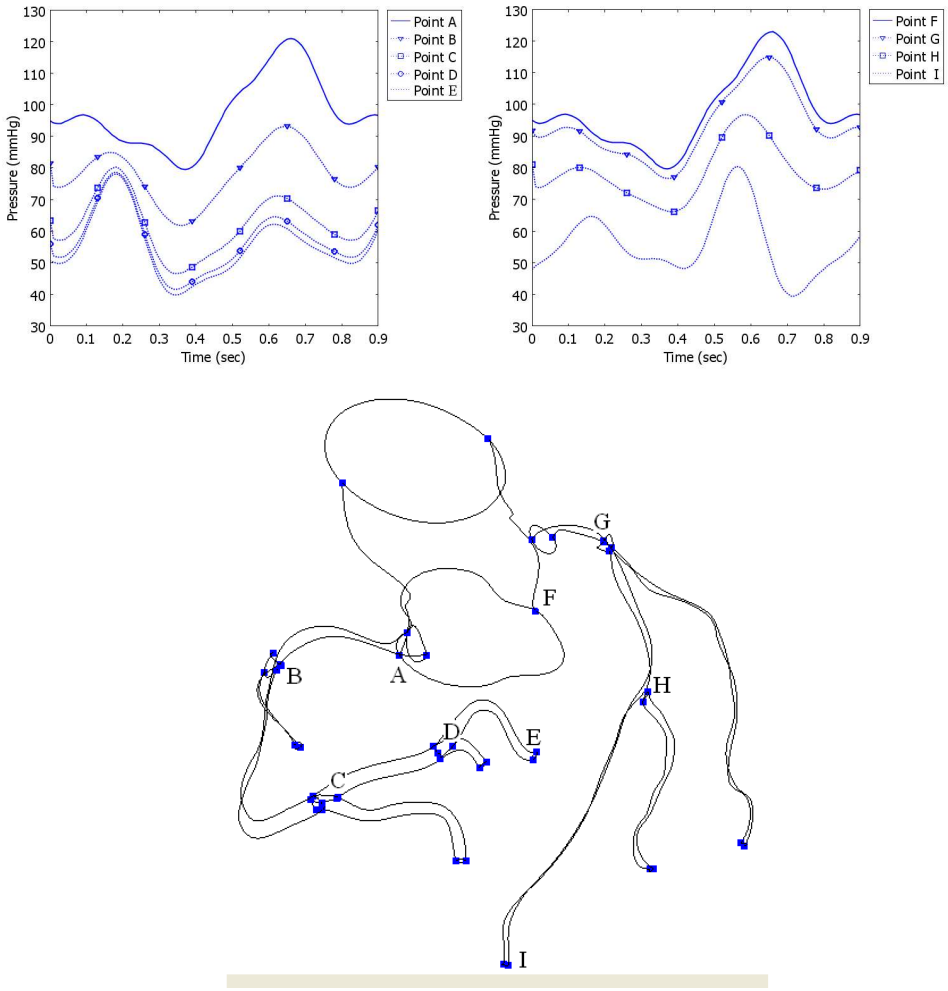

FIGURE 6. Pressure field in a cardiac cycle at various points (A-I) in the RCA and the LCA.

To investigate the branchings on blood flow in the system of human coronary arteries, pressure distribution, velocity field, flow rate and wall shear stress are investigated. Figure 8 shows distributions of blood pressure in the system of coronary arteries with no branch and with branches at the beginning and the peak of the systolic period. Figures 9 and 10 present pressure profiles along the main arteries of the RCA and the LCA connecting to LAD. The figures indicate that blood pressures in the system with branches are significantly less than the ones in the system with no branch. Figures 11 and 12 show the transient flow rate through the main arteries of the RCA and the LCA with branches and with no branch, respectively. It can be noted that the model with branches gives a higher flow rate of blood passing through the main artery with branches. Figures 13 and 14 show the wall shear stresses along the main arteries of the RCA and the LCA connecting to LAD, respectively. Compared with the results obtained from the model with no branch,

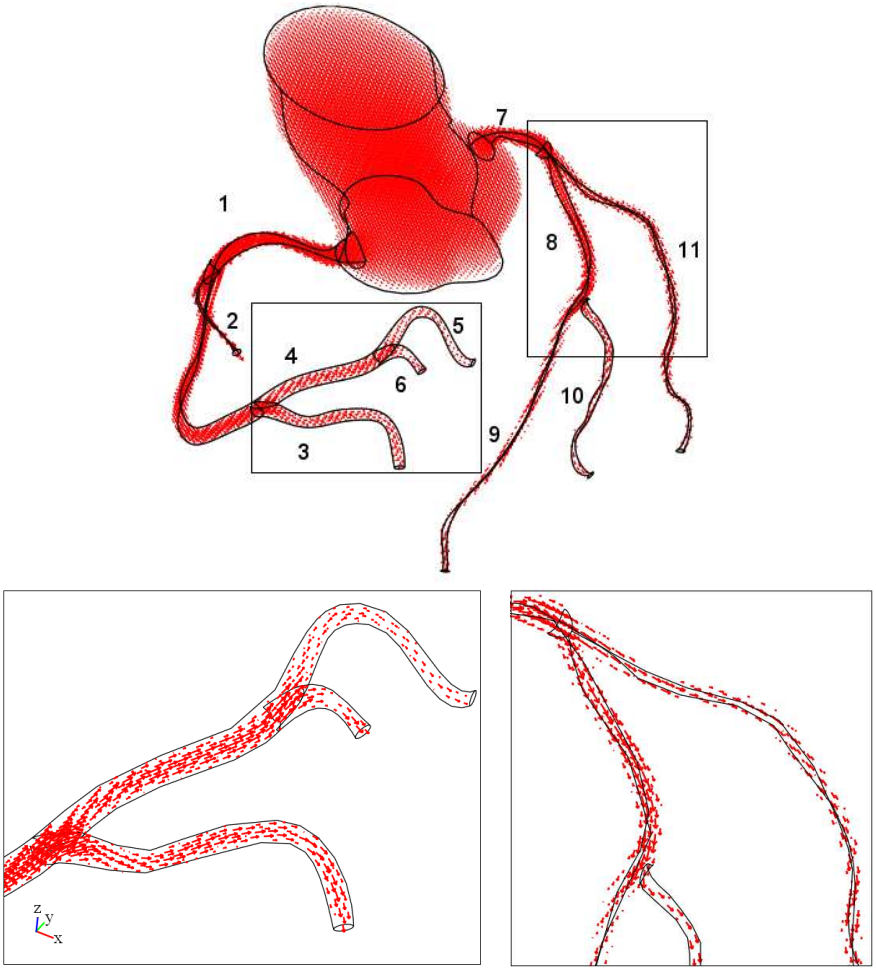

(a) (b)

FIGURE 7. The distribution of blood velocity (cm/sec) from the base of the Aorta to the RCA and the LCA: (a) at the end part of the RCA; (b) the middle part of the LCA.

the wall shear stress tends to increase in the model with branches. The figures depict the appearance of the high wall shear stress around the bifurcation area of the model with branches but at the end of the model with no branches. It has been reported that swirling of a fluid with reverse streamlines occurs when the fluid flows through an obstacle, a curvature, or a region with diameter change [24]. Our results also show that wall shear stress vanishes at some points where swirling flow occurs. Figures 15 and 16 show blood speed during a cardiac cycle at the entrance (the beginning from the aorta of the heart) and at the end of the main arteries of the model with branches and with no branch. In the model with branches, the blood passes through the RCA with the highest speeds of 40 cm/sec at the entrance (solid line) and 5 cm/sec at the end (solid line with square) of the artery as shown

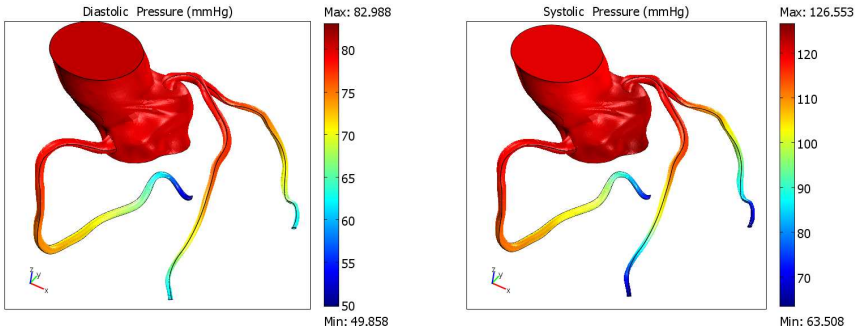

(a)

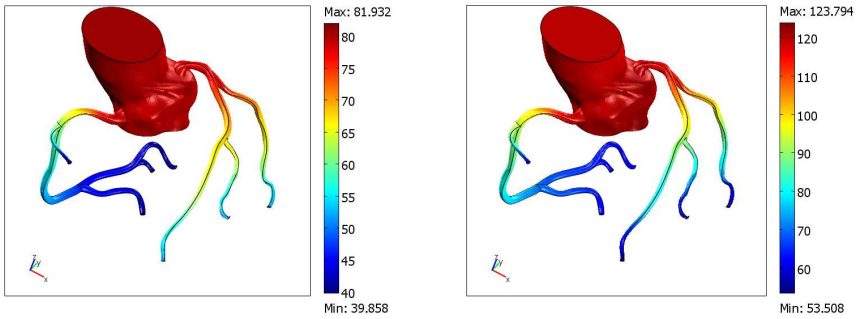

(b)

FIGURE 8. Blood pressure (mmHg) at the beginning (left column) and the peak (right column) of the systolic period in the system of coronary artery: (a) with no branch; (b) with branch.

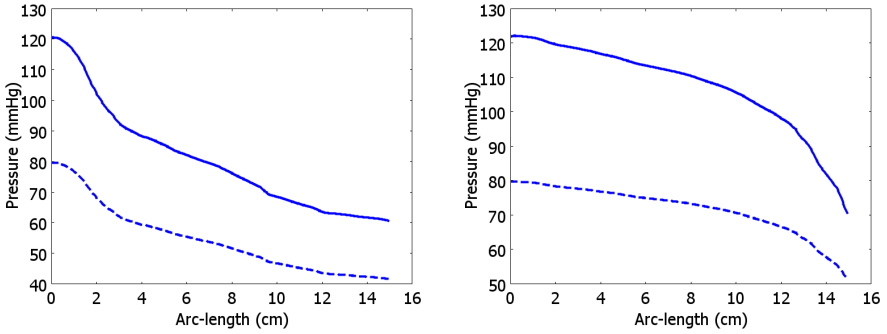

(a) with branches (b) with no branch

FIGURE 9. Pressure along the main artery of the RCA at the beginning (dashed line) and the peak (solid line) of the systolic period: (a) with branch, (b) with no branch.

in Figure 15(a). In the model with no branch, the blood passes through the RCA with the highest speed of 42.5 cm/sec at the entrance of the RCA and it flows with

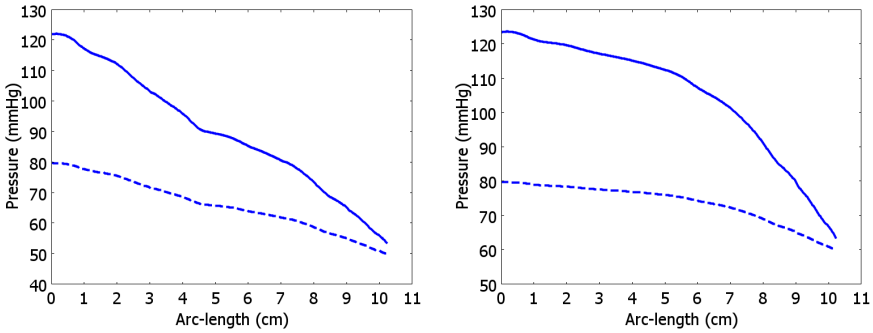

(a) with branches (b) with no branch

FIGURE 10. Pressure along the main artery of the LCA connecting to LAD at the beginning (dashed line) and the peak (solid line) of the systolic period: (a) with branch, (b) with no branch.

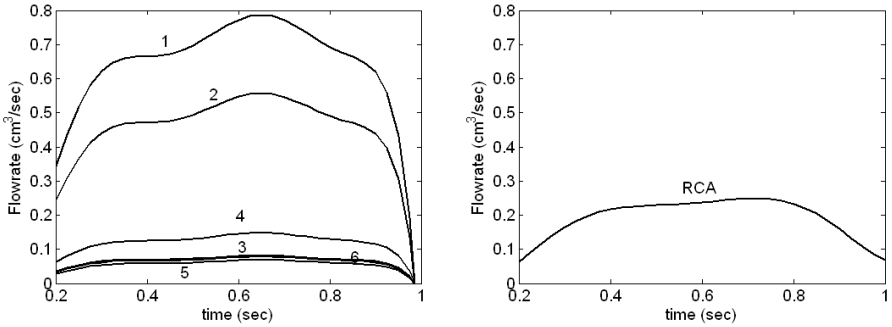

(a) with branches (b) with no branch

FIGURE 11. Transient flow rate through the main artery of the RCA at various locations: (a) with branches, (b) with no branch. The labels 1-6 refer to the locations shown in Figure 7.

the highest speed of 17.5 cm/sec when it arrives to the end of the artery as shown in Figure 15(b). The results also indicate that in the LCA connecting to the LAD with branches, the blood passes through the main artery with the highest speeds of 33 cm/sec at the entrance and 25 cm/sec at the end of the artery as shown in Figure 16(a). In the model with no branch, blood passes through the main artery with highest speeds of 30 cm/sec at both the entrance and at the end of the artery as shown in Figure 16(b).

5. **Conclusions.** In this work, we present the simulation results of the blood flow through the system of the coronary arteries taking into account the pulsatile conditions at the boundaries. The effect of branchings of the artery on the flow problem is investigated. The blood is assumed to be an incompressible non-Newtonian fluid. From the results, it is noted that a branching is a key factor contributing to a reduction in the pressure distribution and an increase in the wall shear stresses along the artery axis. The results show that the branchings of the artery have significant

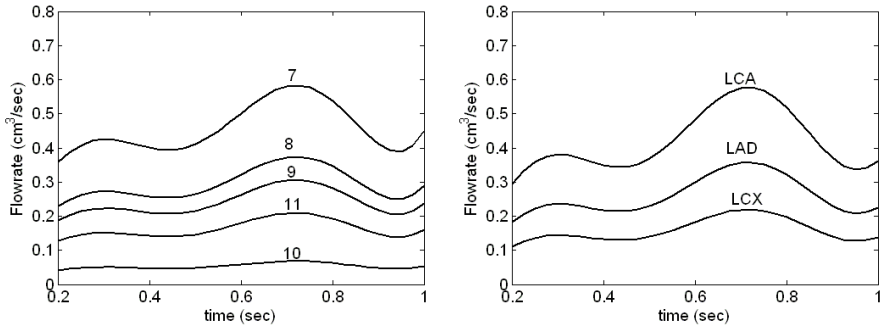

(a) with branches (b) with no branch

FIGURE 12. Transient flow rate through the main artery of the LCA connecting to LAD at various locations: (a) with branches, (b) with no branch. The labels 7-10 refer to the locations shown in Figure 7.

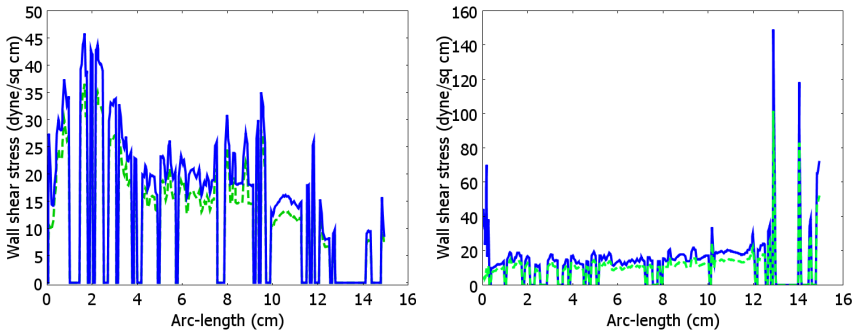

(a) with branches (b) with no branch

FIGURE 13. Wall shear stresses along the main arteries of the RCA at the beginning (dashed line) and the peak (solid line) of the systolic period: (a) with branch, (b) with no branch.

effects on the blood flow. Artherosclerotic lessions may develop due to the higher wall shear stresses at the bifurcation.

Acknowledgments. The first author gratefully acknowledges the support of the Office of the Higher Education Commission and the Thailand Research Fund.

REFERENCES

[1] V. Fuster, R. W. Alexander and R. A. O'Rourke, "Hurst's the Heart," 10^{th} edition, McGraw-Hill, 2001.

[2] L. Ai and K. Vafai, *A coupling model for macromolecule transport in a stenosed arterial wall*, Int. J. Heat Mass Transfer, **49** (2006), 1568–1591.

[3] G. Anastasi, G. Cutroneo, F. Tomasello, S. Lucerna, A. Vitetta, P. Bramanti, P. Di Bella, A. Parenti, A. Porzionato, V. Macchi and R. De Caro, *In vivo basal ganglia volumetry through application of NURBS models to MR images*, Neuroradiology, **48** (2006), 338–345.

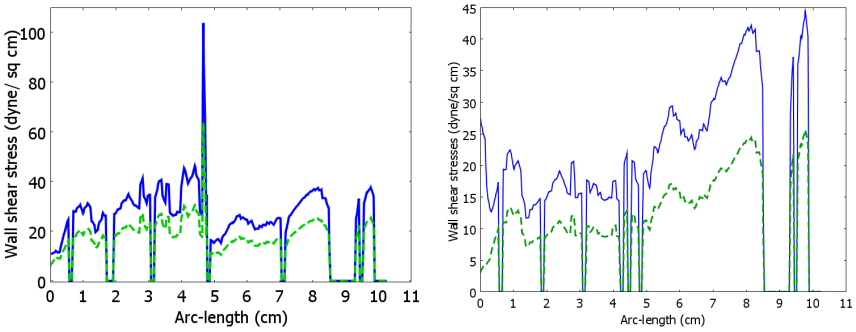

(a) with branches (b) with no branch

FIGURE 14. Wall shear stresses along the main artery of the LCA connecting to LAD at the beginning (dashed line) and the peak (solid line) of the systolic period: (a) with branch, (b) with no branch.

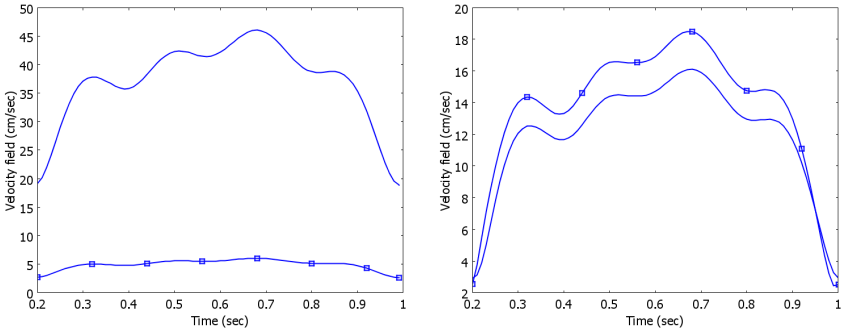

(a) with branches (b) with no branch

FIGURE 15. Velocity field at the entrance (solid line) and at the end (solid line with square) of the main artery of the RCA during a cardiac cycle.

[4] F. G. Basombrío, E. A. Dari, G. C. Buscaglia and R. A. Feijóo, *Numerical experiments in complex hemodynamic flows. Non-Newtonian effects*, XI Congress on Numerical Methods and their Applications (San Carlos de Bariloche, 2000), Int. J. of Computational Fluid Dynamics, **16** (2002), 231–246.

[5] C. Bertolotti and V. Deplano, *Three-dimensional numerical simulations of flow through a stenosed coronary bypass*, J. Biomech., **33** (2000), 1011–1022.

[6] J.-J. Chiu and S. Chien, *Effects of disturbed flow on vascular endothelium: Pathophysiological basis and clinical perspectives* Physiological Review, **91** (2011), 327–387.

[7] C. R. Ethier, D. A. Steinman, X. Zhang, S. R. Karpik and M. Ojha, *Flow waveform effects on end-to-side anastomotic patterns*, J. Biomech., **31** (1998), 609–617.

[8] D. Y. Fei, J. D. Thomas and S. E. Rittgers, *The effect of angle and flow rate upon hemodynamics in distal vascular graft anastomoses: A numerical model study*, J. Biomech Eng., **116** (1994), 331–316.

[9] Z. J. Huang and J. M. Tarbell, *Numerical simulation of mass transfer in porous media blood vessel walls*, Am. J. Physiol Heart Circ Physiol., (1997), 464–477.

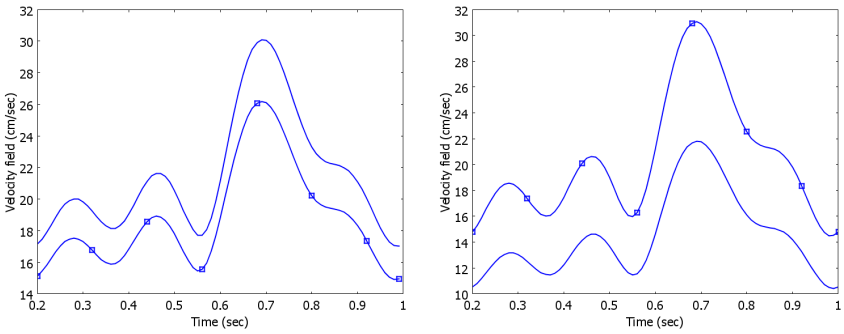

(a) with branches (b) with no branch

FIGURE 16. Velocity field at the entrance (solid line) and at the end (solid line with square) of the main artery of the LCA connecting to the LAD during a cardiac cycle.

[10] J. Chen and X. Y. Lu, *Numerical investigation of non-Newtonian blood flow in a bifurcation model with non-planar branch*, J. Biomech., **37** (2004), 1899–1911.

[11] B. M. Johnston, P. R. Johnstona, S. Corney and D. Kilpatrick, *Non-Newtonian blood flow in human right coronary arteries: Steady state simulations*, J. Biomech., **34** (2004), 709–720.

[12] G. Karner and K. Perktold, *Effect of endothelial injury and increased blood flow pressure on albumin accumulation in the arterial wall: A numerical study*, J Biomech., **33** (2000), 709–715.

[13] D. K. Stangeby and E. R. Ethier, *Computational analysis of coupled blood-wall arterial LDL transport*, J. Biomech Eng., **124** (2002), 1–8.

[14] N. Kowalczyk and J. D. Mace, "Radiographic Pathology for Technologists," MOSBY Elsevier, United States, 2009.

[15] Y. Papaharilaou, D. J. Doorly and S. J. Sherwin, *The influence of out-of-plane geometry on pulsatile flow within a distal end-to-side anatomosis*, J. Boimech., **35** (2002), 1225–1239.

[16] A. Quarteroni and L. Formaggia, *Mathematical modelling and numerical simulation of the cardiovascular system*, in "Handbook of Numerical Analysis" (eds. P. G. Ciarlet and J.-L. Lions), Vol. XII, North-Holland, Amsterdam, (2004), 3–127.

[17] N. H. Staalsen, M. Ulrich, W. Y. Kim, E. M. Pedersen, T. V. How and J. M. Hasenkam, *In vivo analysis and three-dimensional visualization of blood flow patterns at vascular end-to-side anastomoses*, Eur. J. Vasc Endovasc Surg., **10** (1995), 168–181.

[18] S. Tada and J. M. Tarbell, *Interstital flow through the internal elastic lamina affects shear stress on arterial smooth muscle cells*, Am. J. Physiol Heart Circ. Physiol., **278** (2000), 1589–1597.

[19] D. Tang, C. Yang, S. Kobayashi and D. N. Ku, *Steady flow and wall compression in stenotic arteries: A three-dimensional thick-wall model with fluid-wall interactions*, J. Biomech Eng., **123** (2001), 548–557.

[20] R. C. Ward, M. W. Yambert, R. J. Toedte, N. B. Munro, C. E. Easterly, E. P. Difilippo and D. C. Stallings, *Creating a human phantom for the virtual human program*, Stud. Health Technol. Inform., **70** (2000), 368–374.

[21] B. Wiwatanapataphee, D. Poltem, Y. H. Wu and Y. Lenbury, *Simulation of pulsatile flow of blood in stenosed coronary artery bypass with graft*, Math Biosci Eng., **3** (2006), 371–383.

[22] F. G. Basombrío, E. A. Dari, G. C. Buscaglia and R. A. Feijóo, *Numerical experiments in complex hemodynamic flows. Non-Newtonian effects*, Int. J. of Computational Fluid Dynamics, **16** (2002), 231–246.

[23] C. Bertolotti and V. Deplano, *Three-dimensional numerical simulations of flow through a stenosed coronary bypass,* J. Biomech., **33** (2000), 1011–1022.

[24] J.-J. Chiu and S. Chien, *Effects of disturbed flow on vascular endothelium: Pathophysiological basis and clinical perspectives* Physiological Review, **91** (2011), 327–387.

[25] C. R. Ethier, D. A. Steinman, X. Zhang, S. R. Karpik and M. Ojha, *Flow waveform effects on end-to-side anastomotic patterns*, J. Biomech., **31** (1998), 609–617.
[26] D. Y. Fei, J. D. Thomas and S. E. Rittgers, *The effect of angle and flow rate upon hemodynamics in distal vascular graft anastomoses: A numerical model study*, J. Biomech Eng., **116** (1994), 331–316.
[27] Z. J. Huang and J. M. Tarbell, *Numerical simulation of mass transfer in porous media blood vessel walls*, Am. J. Physiol Heart Circ. Physiol., (1997), 464–477.
[28] J. Chen and X. Y. Lu, *Numerical investigation of non-Newtonian blood flow in a bifurcation model with non-planar branch*, J. Biomech., **37** (2004), 1899–1911.
[29] B. M. Johnston, P. R. Johnstona, S. Corney and D. Kilpatrick, *Non-Newtonian blood flow in human right coronary arteries: Steady state simulations*, J. Biomech., **34** (2004), 709–720.
[30] G. Karner and K. Perktold, *Effect of endothelial injury and increased blood flow pressure on albumin accumulation in the arterial wall: A numerical study*, J. Biomech., **33** (2000), 709–715.
[31] D. K. Stangeby and E. R. Ethier, *Computational analysis of coupled blood-wall arterial LDL transport*, J. Biomech Eng., **124** (2002), 1–8.
[32] N. Kowalczyk and J. D. Mace, "Radiographic Pathology for Technologists," MOSBY Elsevier, United States, 2009.
[33] Y. Papaharilaou, D. J. Doorly and S. J. Sherwin, *The influence of out-of-plane geometry on pulsatile flow within a distal end-to-side anatomosis*, J. Boimech., **35** (2002), 1225–1239.
[34] A. Quarteroni and L. Formaggia, *Mathematical modelling and numerical simulation of the cardiovascular system*, in "Handbook of Numerical Analysis" (eds. P. G. Ciarlet and J.-L. Lions), Elsevier, Amsterdam, 2004.
[35] N. H. Staalsen, M. Ulrich, W. Y. Kim, E. M. Pedersen, T. V. How and J. M. Hasenkam, *In vivo analysis and three-dimensional visualization of blood flow patterns at vascular end-to-side anastomoses*, Eur. J. Vasc. Endovasc. Surg., **10** (1995), 168–181.
[36] S. Tada and J. M. Tarbell, *Interstital flow through the internal elastic lamina affects shear stress on arterial smooth muscle cells*, Am. J. Physiol Heart Circ. Physiol., **278** (2000), 1589–1597.
[37] D. Tang, C. Yang, S. Kobayashi and D. N. Ku, *Steady flow and wall compression in stenotic arteries: A three-dimensional thick-wall model with fluid-wall interactions*, J. Biomech Eng., **123** (2001), 548–557.
[38] R. C. Ward, M. W. Yambert, R. J. Toedte, N. B. Munro, C. E. Easterly, E. P. Difilippo and D. C. Stallings, *Creating a human phantom for the virtual human program*, Stud. Health Technol. Inform., **70** (2000), 368–374.
[39] B. Wiwatanapataphee, D. Poltem, Y. H. Wu and Y. Lenbury, *Simulation of pulsatile flow of blood in stenosed coronary artery bypass with graft*, Math Biosci Eng., **3** (2006), 371–383.

Received October 15, 2010; Accepted July 23, 2011.

E-mail address: scbww@mahidol.ac.th
E-mail address: Y.Wu@curtin.edu.au
E-mail address: thanongchai@gmail.com
E-mail address: g5136161@student.mahidol.ac.th